The Journal of Immunology

RESEARCH ARTICLE | AUGUST 15 2016

Structure of the Adenovirus Type 4 (Species E) E3-19K/HLA-A2 Complex Reveals Species-Specific Features in MHC Class I Recognition FREE

Lenong Li; ... et. al

J Immunol (2016) 197 (4): 1399–1407.
https://doi.org/10.4049/jimmunol.1600541

Structure of the Adenovirus Type 4 (Species E) E3-19K/HLA-A2 Complex Reveals Species-Specific Features in MHC Class I Recognition

Lenong Li,* Bernard D. Santarsiero,[†,‡] and Marlene Bouvier*

Adenoviruses (Ads) subvert MHC class I Ag presentation and impair host anti-Ad cellular activities. Specifically, the Ad-encoded E3-19K immunomodulatory protein targets MHC class I molecules for retention within the endoplasmic reticulum of infected cells. We report the x-ray crystal structure of the Ad type 4 (Ad4) E3-19K of species E bound to HLA-A2 at 2.64-Å resolution. Structural analysis shows that Ad4 E3-19K adopts a tertiary fold that is shared only with Ad2 E3-19K of species C. A comparative analysis of the Ad4 E3-19K/HLA-A2 structure with our x-ray structure of Ad2 E3-19K/HLA-A2 identifies species-specific features in HLA-A2 recognition. Our analysis also reveals common binding characteristics that explain the promiscuous, and yet high-affinity, association of E3-19K proteins with HLA-A and HLA-B molecules. We also provide structural insights into why E3-19K proteins do not associate with HLA-C molecules. Overall, our study provides new information about how E3-19K proteins selectively engage with MHC class I to abrogate Ag presentation and counteract activation of CD8$^+$ T cells. The significance of MHC class I Ag presentation for controlling viral infections, as well as the threats of viral infections in immunocompromised patients, underline our efforts to characterize viral immunoevasins, such as E3-19K. ***The Journal of Immunology*****, 2016, 197: 1399–1407.**

Human adenoviruses (Ads) are common pathogens comprising ≥70 types (Ad1–Ad70) classified into seven species (A–G) (1–3). Ads cause a variety of clinical symptoms involving the gastrointestinal, upper respiratory, and ocular systems (4). Although healthy adults can generally control the virus, a large number of infected individuals develop persistent lifelong infections. In immunocompromised individuals, such as children, transplant recipients, and AIDS patients, Ad infections can be severe and even fatal (5–9). The ability of Ad to persist in infected cells presupposes that the virus is capable of interfering with host antiviral cellular immune responses. Consistent with this, it was shown that the E3-19K protein, the most abundantly expressed protein of the early transcription unit 3 of Ads, modulates host immune functions (10, 11). E3-19K binds to and retains MHC class I (MHCI) molecules within the endoplasmic reticulum (ER) of infected cells (10–14). Specifically, the ER lumenal domain of E3-19K associates with the ER lumenal domain of MHCI (15–22), whereas the transmembrane domain of E3-19K and the dilysine motif in its cytoplasmic tail provide signals for sequestration of the E3-19K/MHCI complex within the ER (12–14, 23). As a consequence, Ad-infected human and mouse cells have an impaired ability to present MHCI-associated viral peptides, making infected cells less sensitive to lysis by CTLs (15, 24–28). In animal models, it was shown that E3-19K–mediated effects alter host inflammatory responses to the virus (29, 30). Taken together, in vitro and in vivo data strongly support an immunomodulatory role for E3-19K during human Ad infections.

We determined previously the three-dimensional structure of the Ad type 2 (Ad2) of species C E3-19K/HLA-A2 complex (31). The structure showed that Ad2 E3-19K adopts a novel tertiary fold and uses a new binding surface on HLA-A2. We set out to characterize how the structure of E3-19K and its mode of interaction with HLA-A2 vary among Ad species. This is an intriguing question given that all E3-19K proteins characterized thus far have an MHCI-binding function, but their ER lumenal domains share only ∼35% sequence homology across Ad species. Furthermore, we (16, 32–34) showed that the affinities of E3-19K proteins for a given MHCI molecule of the HLA-A and HLA-B loci vary significantly across Ad species and that, interestingly, E3-19K proteins do not associate with HLA-C molecules. The locus-specific recognition and down-regulation of MHCI molecules by other viral immunomodulatory proteins were reported previously (35–39). Presumably, such strategies allow virally infected cells to escape recognition by CD8$^+$ TCRs while also preventing activation of NK cell–inhibitory receptors that recognize HLA-C molecules (missing "self") (37, 39).

To advance our understanding of how the amino acid sequences of Ad E3-19K proteins affect their tertiary structures and interaction with MHCI molecules, as well as to gain insights into the molecular basis for their selective recognition of MHCI, we determined the x-ray crystal structure of Ad type 4 (Ad4) (species E) E3-19K bound to HLA-A2. An analysis of the structure allows us to identify similarities and differences in the binding modes of Ad4 and Ad2 E3-19K, as well as common and unique contact sites on HLA-A2. Moreover, from our results, we make some predictions on the structures of E3-19K proteins

*Department of Microbiology and Immunology, College of Medicine, University of Illinois, Chicago, IL 60612; [†]Department of Medicinal Chemistry and Pharmacognosy, College of Pharmacy, University of Illinois, Chicago, IL 60612; and [‡]Center for Biomolecular Sciences, College of Pharmacy, University of Illinois, Chicago, IL 60607

ORCID: 0000-0002-9032-9699 (B.D.S.).

Received for publication March 29, 2016. Accepted for publication June 2, 2016.

This work was supported in whole or in part by National Institute of Allergy and Infectious Diseases Grants R01AI108546 and R03AI114611 (to M.B.) and National Center for Complementary and Alternative Medicine Grant 1U41AT008706 (to B.D.S.).

The atomic coordinates and structure factors presented in this article have been submitted to the Protein Data Bank (http://www.rcsb.org/pdb/home/home.do) under accession number 5IRO.

Address correspondence and reprint requests to Dr. Marlene Bouvier, Department of Microbiology and Immunology, College of Medicine, University of Illinois, Chicago, IL 60612. E-mail address: mbouvier@uic.edu

The online version of this article contains supplemental material.

Abbreviations used in this article: Ad, adenovirus; Ad2, Ad type 2; Ad4, Ad type 4; ER, endoplasmic reticulum; β_2m, β_2-microglobulin; MHCI, MHC class I; Sc, shape complementarity coefficient.

of species B and D, which have not yet been determined. Overall, our study provides new molecular insights into how Ad uses its E3-19K proteins to selectively subvert MHCI Ag presentation, with implications on disabling $CD8^+$ T cell and NK cell activities.

Materials and Methods

Cloning and protein expression

The cDNA encoding the ER lumenal domain (residues 1–108) of Ad4 E3-19K was generated by PCR, as described previously (33). Plasmids harboring the DNA sequences for HLA-A*0201 H chain (residues 1–275) and β_2-microglobulin (β_2m) (residues 0–99) were kind gifts of Dr. Don C. Wiley (deceased). Ad4 E3-19K, HLA-A2 H chain, and β_2m were expressed in the *Escherichia coli* strain BL21(DE3)pLysS (Stratagene, La Jolla, CA) as inclusion bodies. Inclusion bodies were purified from cell pellets and solubilized as described previously (40).

In vitro assembly of HLA-A2/Tax and Ad4 E3-19K/HLA-A2

HLA-A2/Tax was reconstituted from the urea-solubilized inclusion bodies of HLA-A2 H chain (1 μM) and β_2m (2 μM) in the presence of the Tax peptide (LLFGYPVYV) (10 μM) in an oxidative refolding buffer (40). Stock solutions of purified HLA-A2/Tax (10–30 mg/ml) in 20 mM Tris-HCl (pH 7.5), 150 mM NaCl were kept at −80°C. The Ad4 E3-19K/HLA-A2 complex was assembled using a modified version of this approach, as we described previously (31). Briefly, the urea-solubilized inclusion bodies of Ad4 E3-19K were added at 4°C under rapid stirring, to a final concentration of 1 μM, into an oxidative refolding buffer containing a submolar amount (0.2 μM) of refolded, purified HLA-A2/Tax. The refolding mixture was incubated at 4°C. After 24 h, the mixture was concentrated in an Amicon stirred cell, followed by purification of the mixture on a Superdex 200 HR 10-30 column in 20 mM Tris-HCl (pH 7.5), 100 mM NaCl. The purified Ad4 E3-19K/HLA-A2 complex generated from this rescue refolding strategy migrated as three distinct bands on $NaDodSO_4$ PAGE gel and as a single compact band on native PAGE gel. Stock solutions of purified Ad4 E3-19K/HLA-A2 (20-40 mg/ml) in 20 mM Tris-HCl (pH 7.5), 100 mM NaCl were kept at −80°C.

Native gel band-shift assay

Samples of Ad4 and Ad2 E3-19K proteins (13 μg) were incubated on ice with HLA-A2 and HLA-A2 mutants (20 μg) (2:1 molar ratio) in 20 mM Tris-HCl (pH 7.5) and 150 mM NaCl for 30 min. The mixtures were loaded onto a native PAGE gel (10%) and run at 4°C in 25 mM Tris-HCl (pH 8.4) and 200 mM glycine. Proteins were visualized with Coomassie blue R-250. Note that the isoelectric point of Ad2 E3-19K is 8.85; when isoelectric points of proteins are above the pH of the running buffer (pH 8.4), they do not penetrate into the native gel.

Crystallization and x-ray data collection

Crystallization conditions of the Ad4 E3-19K/HLA-A2 complex were set up with the aid of a Tecan Freedom EVO 200 robot using sitting drops. Complex solution (1 μl, 10 mg/ml) was dispensed into each well of a Corning 96-well plate, mixed with an identical volume of precipitant solution, and equilibrated against 100 μl of reservoir solution. The plates were incubated at 18°C. The initial crystallization condition was found using Crystal Screen Index (Hampton Research) as solution #30, 1.5 M ammonium sulfate, 0.1 M NaCl, and 0.1 M Bis-Tris (pH 6.5). Optimization of the crystallization condition was carried out using the Additive Screen (Hampton Research) and the hanging-drop vapor-diffusion method. Crystals used for data collection were grown by mixing 2 μl of 10 mg/ml protein complex solution with 2 μl of 1.5 M ammonium sulfate, 0.1 M NaCl, 0.1 M Bis-Tris (pH 6.5), and 0.2 μl of 30% 1,6-diaminohexane as additive. Crystals grew over 15 d to dimensions ~ 300 × 150 × 100 μm. Prior to data collection, the crystals were soaked for ~1–2 min in mineral oil (Sigma) with 1.5 M ammonium sulfate, 0.1 M NaCl, and 0.1 M Bis-Tris (pH 6.5) as the cryoprotectant and then flash-frozen in liquid nitrogen. X-ray diffraction data for the Ad4 E3-19K/HLA-A2 complex were collected to 2.64-Å resolution with a MAR-225 CCD detector at LS-CAT beamline 21-ID-F of the Advanced Photon Source (Argonne National Laboratory, Argonne, IL). The space group was determined to be P3 (see Table I). Data were processed and scaled with the HKL-2000 program package (41).

Structure determination and refinement

The structure of Ad4 E3-19K/HLA-A2 complex was determined by molecular replacement in AMoRe (42) using free HLA-A2/Tax (PDB 1HHK) as a search model. Six solutions were identified for both the rotation and translation functions, corresponding to six molecules of Ad4 E3-19K/HLA-A2 in the asymmetric unit. After molecular replacement and an initial refinement with REFMAC (CCP4) (43), the electron-density maps were calculated and examined manually using Coot (44); residues with a poor fit to the electron density map were omitted from the model. Subsequent model rebuilding and refinement was carried out in Coot and phenix.refine (45). Phenix.refine was used for several rounds of refinement with the imposition of noncrystallographic symmetry restraints and application of the appropriate twin law (-h,-k, l) with a twin fraction of 0.470, as suggested from Xtriage (45). In the final rounds of refinement, the noncrystallographic symmetry restraints were released, and a composite omit map was calculated to reduce model bias. Water molecules were added and checked with the F_O-F_C electron-density map (>3σ) at ≤3.8 Å from hydrogen bond donors or acceptors. A total of 40 water molecules was added to the model. Throughout refinement, agreement between the model and the observed data was monitored by calculating R_{free} based on 2% of the reflections. The final R_{work} and R_{free} values (with a bulk solvent correction) were 25.7 and 28.8%, respectively, for all reflections between 49.62 and 2.64 Å (Table I). In the final model, the structural geometry was checked using PROCHECK (46). All backbone $\phi-\psi$ torsion angles of the model were within allowed regions of the Ramachandran plot. Because of poor quality or missing electron density, the final model does not include residues 273–275 of chains A, E, I, M, Q, and U; residues 97–100 of chains C, G, K, O, S, and W; residues 1–6 of chain D; and residues 1–5 of chains H, L, P, T, and X. Buried surface areas were calculated with the program AREAIMOL in the CCP4 package, using a probe radius of 1.4 Å. All structural figures were prepared using PyMol (47).

Results

Structure of the Ad4 E3-19K/HLA-A2 complex

The Ad4 E3-19K/HLA-A2 complex was assembled using an in vitro rescue-refolding strategy that we described previously (31). Briefly, the inclusion bodies of Ad4 E3-19K were injected into a refolding buffer containing a submolar amount of HLA-A2/LLFGYPVYV complex; the presence of folded HLA-A2 in the buffer was absolutely necessary to promote formation of Ad4 E3-19K/HLA-A2 complex (see *Materials and Methods*). The structure of Ad4 E3-19K/HLA-A2 was determined to 2.64 Å by molecular replacement from twinned crystals (see *Materials and Methods*, Table I). Only

Table I. X-ray data processing and refinement statistics

Data collection	
Wavelength (Å)	1.00
Space group	P3
Unit cell parameters	
a, b, c (Å)	165.73, 165.73, 122.86
α, β, γ (°)	90.0, 90.0, 120.0
Resolution (Å)	100–2.64 (2.69–2.64)[a]
Unique reflections	110878
Rmerge	0.172 (0.619)[a]
Redundancy	7.9 (6.7)[a]
Completeness (%)	100 (100)[a]
I/σI	23.4 (2.5)[a]
Refinement	
Resolution (Å)	49.62–2.64
R_{work}/R_{free}[b]	0.266/0.285
Twin law (-h, -k, l)	0.47
No. protein atoms	22994
No. water molecules	40
Root-mean-square deviations	
Bond lengths (Å)	0.006
Bond angles (°)	1.2
B-factors (Å^2)	
Protein	57.3
Water	20.7
Ramachandran plot[c]	
Most favored regions (%)	82.1
Allowed regions (%)	16.8
Generously allowed regions (%)	1.1
Disallowed regions (%)	0

[a] Values in parentheses are for the highest-resolution shell.

[b] R_{work} and R_{free} are defined as $\Sigma||Fobs|-|Fcalc||/\Sigma|Fobs|$ for the reflections in the working or the test set, respectively.

[c] As defined by PROCHECK (46).

minor differences were observed between the six molecules of E3-19K in the asymmetric unit (root-mean-square deviation of 0.31–0.39 Å for 103 equivalent Cα atoms), such that only chain B will be discussed. We observed clear electron density for most residues of the structure: residues 6–108 of Ad4 E3-19K, residues 1–271 of HLA-A2 H chain, residues 0–97 of β_2m, and HIV-1 Tax LLFGYPVYV peptide.

The overall structure of the Ad4 E3-19K/HLA-A2 complex is shown in Fig. 1A. Ad4 E3-19K binds at the N-terminal end of the HLA-A2 groove contacting the N terminus of the α1 helix, C terminus of the α2 helix, a loop of the α3-domain, and a β_2m subunit. This mode of binding is reminiscent of the way that Ad2 E3-19K associates with HLA-A2/LLFGYPVYV (31), with unique features (see below).

The Ad4 E3-19K structure (Fig. 1B) consists of a long N terminus segment followed by a large domain formed by two antiparallel β-sheets defined by β-strands A, B, and D and β-strands C, E, and F. The two β-sheets overlap only slightly with each other and adopt a V-shaped arrangement. The N-domain is followed by a short α helix and then a tail segment. There are a number of critical interactions along the entire length of the Ad4 E3-19K structure. First, the three disulfide bonds are strategically positioned (Fig. 1B, 1C): Cys^{10}/Cys^{39} links the long N terminus segment (Lys^6 to Lys^{17}) to the BC-loop (loop connecting β-strands B and C), Cys^{18}/Cys^{35} connects β-strands A and B, and Cys^{29}/Cys^{91} keeps the α helix packed against the large N-domain. Second, a number of residues form a well-defined hydrophobic core (Fig. 1C). These residues are Val^{31} and Ile^{33} (β-strand B) and Leu^{55} (β-strand D) for the ABD β-sheet and Val^{42}, Ile^{44}, and Tyr^{46} (β-strand C), Tyr^{67} and Val^{69} (β-strand E), and Asn^{83} (β-strand F) for the CEF β-sheet. Other residues contributing to the hydrophobic core are Asn^{53}, Trp^{59}, and Asp^{63} of the large N terminus domain, Phe^{87} and Met^{95} of the α helix, and Trp^{104} of the tail. Finally, several hydrogen bonds contribute to the well-ordered electron density of the long N terminus segment (Lys^6–Lys^{17}): the main chain of Pro^9 forms a hydrogen bond with the side chain of Thr^{12}, and the main chain of Asp^{16} forms a hydrogen bond with the side chain of Asn^{83}. A hydrogen bond between the main chain atoms of Ser^{98} and Met^{103} is also critical for stabilizing the α helix against the N terminus domain. Overall, Ad4 E3-19K adopts a similar tertiary fold as Ad2 E3-19K (31), a fold that is unique to this family of proteins, but also shows distinct structural features (see below).

The Ad4 E3-19K/HLA-A2 binding interface

The Ad4 E3-19K/HLA-A2 binding interface shields a molecular surface area of 2112 $Å^2$ from solvent. The shape complementarity coefficient (Sc) of the complex was determined to be 0.66 (Sc = 1 for perfect geometrical fits) (49). We divided the overall binding interface into four sites (sites 1–4) (Fig. 2). Site 1, located at the N terminus of the α1 helix on HLA-A2, is defined by numerous hydrophobic contacts involving Gln^{23} (β-strand A), Trp^{37} (BC-loop), and Thr^{54} and Ala^{56} (β-strand D) of E3-19K and a number of HLA-A2 H chain residues. Site 2, located at the C terminus of the α2 helix on HLA-A2, is characterized by a few hydrogen bonds mediated by Lys^{49} and Arg^{51} (CD-loop) and Ala^{56} (β-strand D)

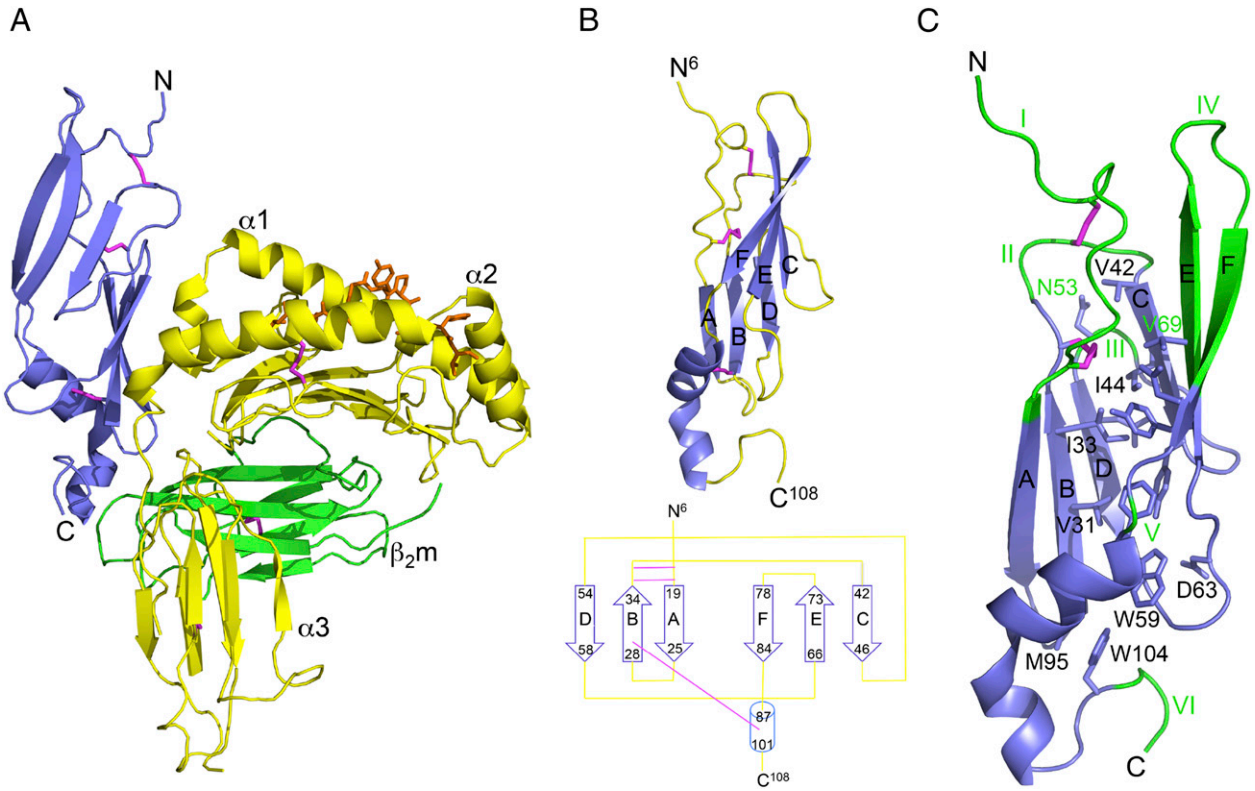

FIGURE 1. The structure of Ad4 E3-19K/HLA-A2. (**A**) Ribbon representation of the Ad4 E3-19K/HLA-A2 structure: E3-19K, slate; HLA-A2 H chain (α1-, α2-, and α3-domains), yellow; β_2m, green; HIV-1 Tax peptide (LLFGYPVYV), orange; and disulfide bonds, magenta. The N and C termini of Ad4 E3-19K are labeled. (**B**) Ribbon representation of the complex structure of Ad4 E3-19K (upper panel) and topology diagram (lower panel). The N-terminal domain (residues 6–86), α helix (residues 87–101), and tail (residue 102–108) are indicated. The β-strands are represented with arrows, and α helix is represented as a cylinder. The β-strands and N^6- and C^{108}-termini are labeled. (**C**) Ribbon representation of the complex structure of Ad4 E3-19K showing the side chains of hydrophobic core-forming residues (slate) (only some side chains were labeled for clarity). Core-forming residues (>90% buried) were determined by SPDBV (48). The β-strands and N and C termini are labeled. The regions of major conformational differences (root-mean-square deviation > 2.5 Å) between Ad4 E3-19K and Ad2 E3-19K (superimposition of Ad4 E3-19K/HLA-A2 and Ad2 E3-19K/HLA-A2) are green and labeled I–VI (see also the legend for Fig. 3A).

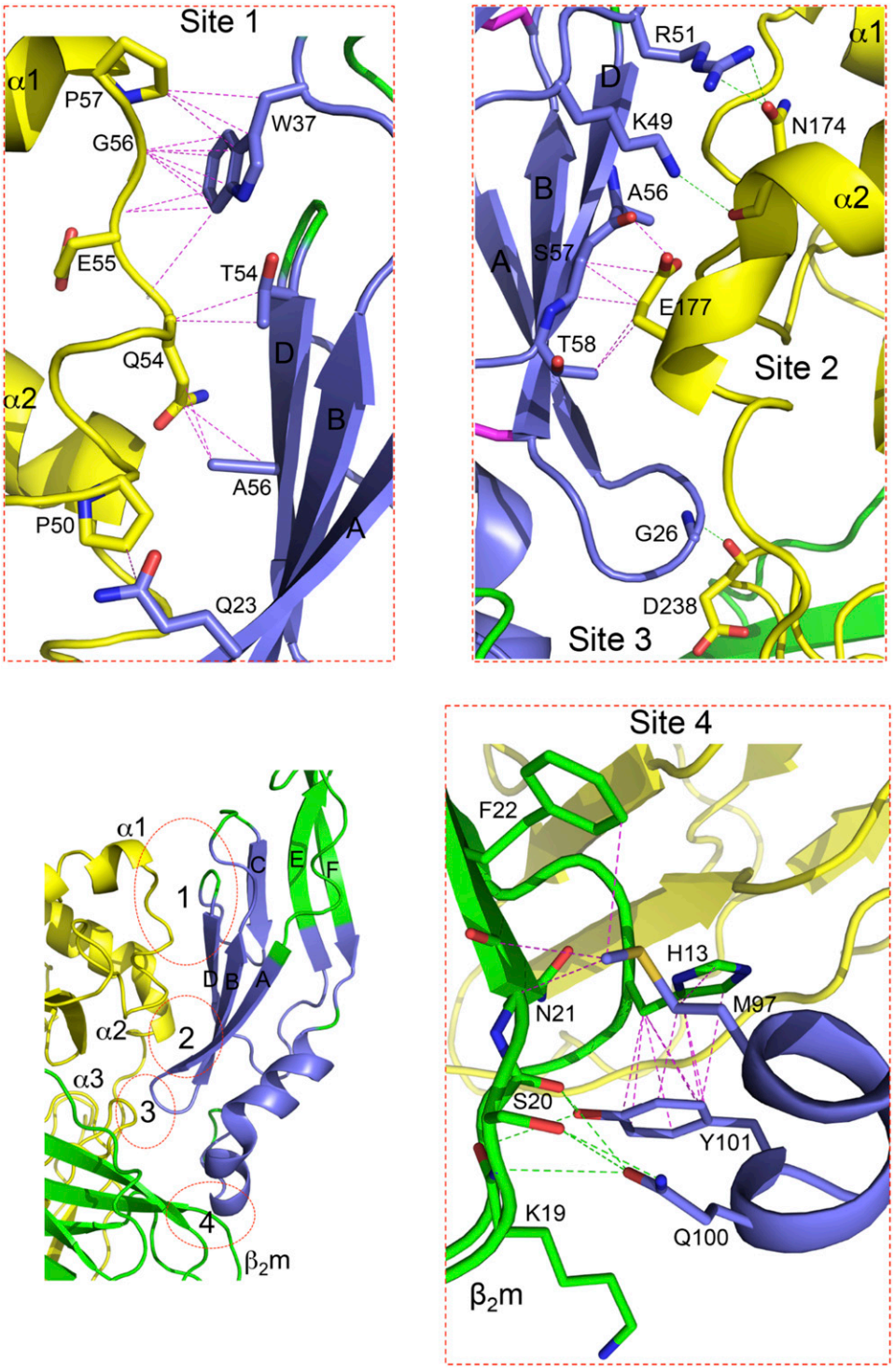

FIGURE 2. Interaction surface between Ad4 E3-19K and HLA-A2. Interactions at sites 1–4 of Ad4 E3-19K/HLA-A2 are shown as an overview (lower left panel) and as three enlargements (same color code as in Fig. 1A). Nitrogen and oxygen atoms are blue and red, respectively. Hydrogen bonds (distance $\leq$ 3.5 Å) are indicated by dashed green lines, and hydrophobic contacts (distance $<$ 4.0 Å) are represented by dashed magenta lines. The β-strands of Ad4 E3-19K, the α1-, α2-, and α3-domains of HLA-A2 H chain, and β_2m are labeled.

of E3-19K and Asn[174] and Glu[177] of HLA-A2 H chain. A number of hydrophobic contacts also contribute to site 2. Site 3 is more localized and consists of a hydrogen bond between Gly[26] (AB-loop) of E3-19K and Asp[238] of the α3-domain of HLA-A2 H chain. Finally, site 4 is defined by hydrogen bonds involving Gln[100] and Tyr[101] (α helix) of E3-19K and Lys[19] and Ser[20] of β_2m. This region is also characterized by numerous hydrophobic contacts.

The Ad4 E3-19K versus Ad2 E3-19K structures

An alignment of the Ad4 and Ad2 E3-19K amino acid sequences (Fig. 3A) shows that, although the ER lumenal domains of Ad4 and Ad2 E3-19K proteins share only 36% sequence identity (residue marked in red in Fig. 3A), their overall complex structures are very similar (Fig. 3B, Ad4 E3-19K structure serves as the reference). There are 36 strictly (red) and 9 highly (pink) conserved residues (Fig. 3A) that are distributed along the entire length of the structures (Fig. 3B), clustering especially on β-strand B and DE-loop of the large domain, α helix, and tail. Remarkably, the majority (~70%) of residues that make up the hydrophobic core in Ad4 and Ad2 structures (see Fig. 1C, and residues marked with an asterisk in Fig. 3A) are strictly and highly conserved. Therefore, the hydrophobic core is critical for conservation of the E3-19K tertiary fold; accordingly, regions with the largest differences between the two structures (defined as regions I–VI in

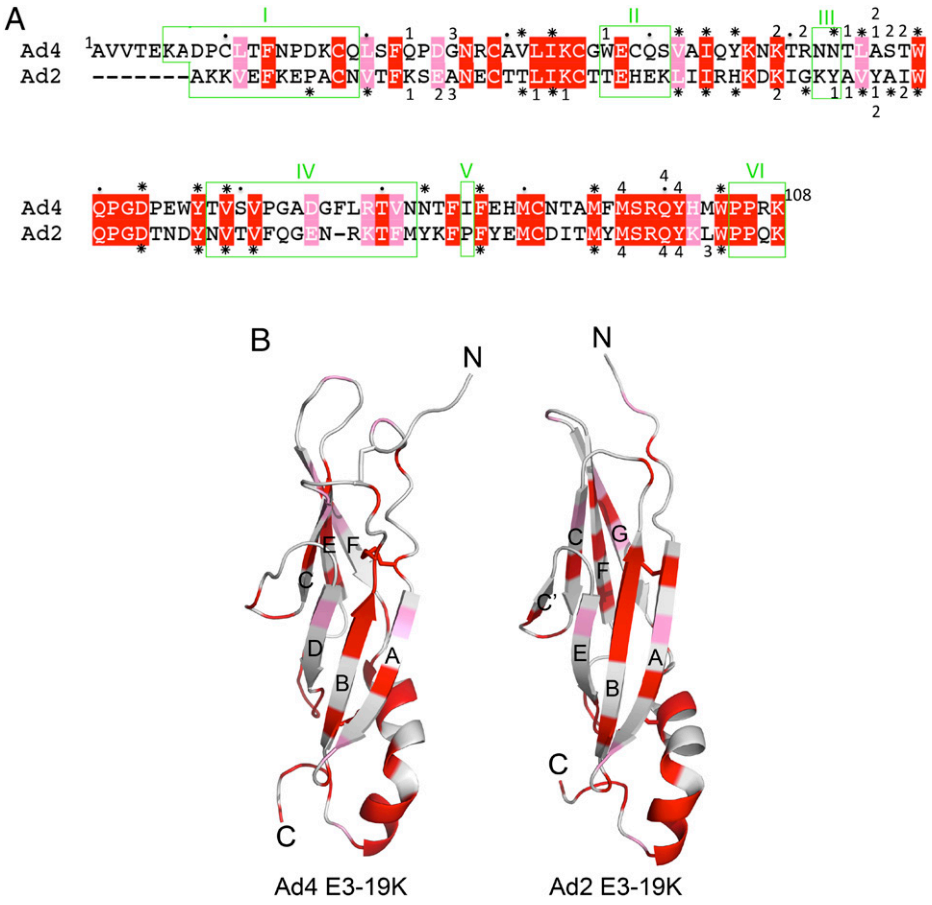

FIGURE 3. Conserved residues in Ad4 and Ad2 E3-19K. (**A**) Amino acid sequence alignment of Ad4 and Ad2 E3-19K. Strictly (red) and highly (pink) conserved residues are indicated: residues in Ad4 and Ad2 E3-19K at interaction sites 1–4 are indicated by numbers, and core-forming residues (> 90% buried) are indicated by an asterisk. Regions of major conformational differences between Ad4 and Ad2 E3-19K are indicated by green boxes labeled I–VI (see also the legend for Fig. 1C). (**B**) Strictly (red) and highly (pink) conserved residues are mapped in the Ad4 and Ad2 E3-19K (31) structures. The β-strands and N and C termini are labeled.

Figs. 1C, 3A) are devoid of core-forming residues, with the exception of Asn[53] and Val[69]. There are four strictly conserved Cys residues in Ad4 and Ad2 E3-19K (Fig. 3A) that form two disulfide bonds (Cys[18]/Cys[35] and Cys[29]/Cys[91]) along β-strand B (Fig. 3B), tethering it to the long N terminus segment and α helix, respectively. These conserved disulfide bonds are critical to the E3-19K fold, as demonstrated previously (50), and their strategic positioning on the ABD β-sheet likely provides conformational rigidity to this face of the proteins. The long N terminus segment of Ad4 E3-19K is tethered to the BC-loop by an additional disulfide bond (Cys[10]/Cys[39]) (Fig. 3B); this disulfide bond is conspicuously absent in Ad2 E3-19K due to a shorter N terminus. Overall, the two E3-19K proteins have similar complex structures owing to the conservation of key structural residues and determinants, as well as their shared MHCI-binding function.

Comparison of the Ad4 E3-19K/HLA-A2 and Ad2 E3-19K/HLA-A2 structures

A comparative analysis of the Ad4 E3-19K/HLA-A2 and Ad2 E3-19K/HLA-A2 structures reveals similarities and differences in the binding mode of E3-19K proteins onto HLA-A2. Fig. 4A (upper left panel) shows a front view of the residues that Ad4 E3-19K (yellow balls) and Ad2 E3-19K (orange balls) interact with on HLA-A2, highlighting how both proteins contact generally the same four regions of HLA-A2. Notably, although a number of HLA-A2 residues that the E3-19K proteins bind to are the same at sites 1, 2, and 4, each protein also has unique contact residues at sites 1 and 2 and, in particular, at site 3 (Fig. 4A). A side view (Fig. 4A, upper right panel) shows how sites 1, 2, and 4 are spatially organized along the interaction surface, with contact residues Gln[54] (site 1) and Glu[177] (site 2) on HLA-A2 H chain and Lys[19] and Ser[20] on β_2m (site 4) occupying prominent positions (see also Fig. 4C). Fig. 4A (lower panel) shows an amino acid sequence alignment of consensus HLA-A, HLA-B, and HLA-C H chains at interaction sites 1–4. The information shows that sites 1 and 2 are composed mostly of conserved MHCI residues, whereas site 3 is composed largely of polymorphic residues. Site 4 involves β_2m residues and, therefore, is strictly conserved in all MHCI molecules. Thus, overall, Ad4 and Ad2 E3-19K proteins contact largely conserved residues on HLA-A2, although not necessarily the same conserved residues (Fig. 4A).

The residues in E3-19K protein that bind at sites 1–4 on HLA-A2 are shown in Fig. 4B. A number of observations can be made (Ad4 E3-19K/HLA-A2 structure serves as the reference). First, all contact residues are found in regions of highest structural similarities between the two structures, with the exception of Trp[37] in Ad4 and Tyr[46] in Ad2. Second, in both structures, the contact residues are located on the ABD β-sheet, in particular along β-strand D, and on the α helix; there are no contact residues on the CEF β-sheet. Third, both E3-19K proteins use primarily nonconserved residues of the large N-domain and loops to associate with HLA-A2 H chain at sites 1–3 (Figs. 3A, 4B). In contrast, both E3-19K proteins use strictly conserved residues of the α helix to interact with β_2m at site 4 (Figs. 3A, 4B); there are only four strictly conserved residues (Lys[49], Met[97], Gln[100], and Tyr[101]) that are used functionally by both E3-19K proteins, further underlining that conservation of residues in E3-19K is primarily to preserve the tertiary fold. Finally, Ala[56] in Ad4 and Tyr[49] in Ad2, which occupy equivalent positions structurally on β-strand D (Fig. 4B), are the only residues in each E3-19K protein that mediate interactions with HLA-A2 H chain at two different sites (1 and 2), bridging the α1 and α2 helices. This further underlines the critical functional role of β-strand D.

It is also noteworthy that both E3-19K proteins make extensive contacts with HLA-A2 residues Gln[54] and Glu[177] (Fig. 4C), which

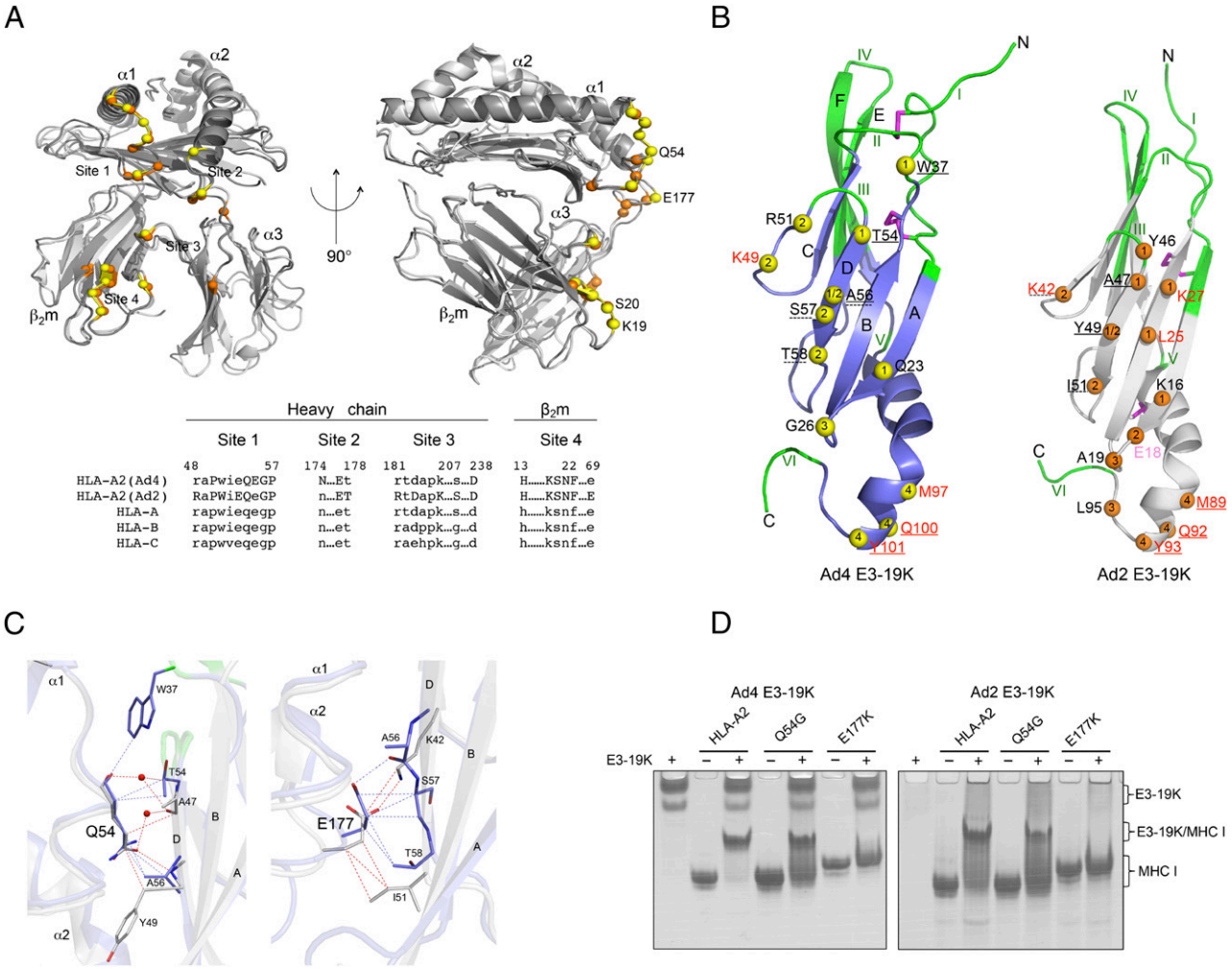

FIGURE 4. Contact residues in Ad4 E3-19K/HLA-A2 and Ad2 E3-19K/HLA-A2 structures. (**A**) Superimposition of Ad4 E3-19K/HLA-A2 and Ad2 E3-19K/HLA-A2 (31) structures (upper panels), in front (upper left panel) and side (upper right panel) views, showing contact residues on HLA-A2 (sites 1–4) for Ad4 E3-19K (yellow balls) and Ad2 E3-19K (orange balls). The side view shows that residues Gln^{54}, Glu^{177}, Lys^{19}, and Ser^{20} occupy prominent positions along the binding interface. The α1-, α2-, and α3-domains of HLA-A2 H chain and β_2m are labeled. Amino acid sequence alignment of HLA-A2 and the consensus HLA-A, HLA-B, and HLA-C H chain sequences (consensus sequences were obtained from the IMGT-HLA Sequence Database [http://www.ebi.ac.uk/imgt/hla/align.html]) at sites 1–3 (lower panel). Uppercase letters designate contact residues at each site. (**B**) Residues in Ad4 E3-19K (yellow balls) and Ad2 E3-19K (orange balls) that contact HLA-A2 at sites 1–4 are indicated with the site numbers. Nonconserved residues are black, strictly conserved residues are red, and the highly conserved residue is pink. Residues in both Ad4 and Ad2 E3-19K interacting with HLA-A2 residue Gln^{54} are denoted by solid black underlines; similarly, residues interacting with HLA-A2 residue Glu^{177} are denoted by dashed black underlines. Strictly conserved residues in both Ad4 and Ad2 E3-19K interacting with β_2m residues Ser^{19} and Lys^{20} are denoted by solid red underlines. Regions of major conformational differences between Ad4 and Ad2 E3-19K are green (see also the legend for Fig. 1C). (**C**) A close-up view of the superimposed Ad4 E3-19K/HLA-A2 (slate) and Ad2 E3-19K/HLA-A2 (gray) (31) structures showing interactions at residues Gln^{54} (left panel) and Glu^{177} (right panel). All interactions are shown as dashed red lines for Ad4 E3-19K/HLA-A2 and dashed blue lines for Ad2 E3-19K/HLA-A2. The α1- and α2-domains of HLA-A2 H chain and β-strands of Ad4 E3-19K (only) are labeled. (**D**) Native gel band-shift assay showing how a single-point mutation at Gln^{54} and Glu^{177} in HLA-A2 H chain impairs interaction with Ad4 E3-19K (left panel) and Ad2 E3-19K (right panel). See *Materials and Methods* for conditions.

occupy striking positions along the binding interface (Fig. 4A, upper right panel). Specifically, Ad4 E3-19K uses Trp^{37}, Thr^{54}, and Ala^{56} to interact with Gln^{54}, whereas Ad2 E3-19K uses Ala^{47} and Tyr^{49} (Fig. 4A, upper left panel; see also the solid black line in Fig. 4B), and Ad4 E3-19K uses Ala^{56}, Ser^{57}, and Thr^{58} to interact with Glu^{177}, whereas Ad2 E3-19K uses Lys^{42} and Ile^{51} (Fig. 4A, upper right panel; see also the dashed black line in Fig. 4B). Overall, this is consistent with HLA-A2 residues Gln^{54} and Glu^{177} playing critical roles at the E3-19K/HLA-A2 interfaces.

MHCI residues 54 and 177 modulate interactions with E3-19K proteins

The above analysis provides a strong rationale for examining the roles of HLA-A2 H chain residues 54 and 177 in modulating interactions with Ad2 and Ad4 E3-19K proteins. We made the single-point mutations Gln^{54} to Gly^{54} (Q54G) and Glu^{177} to Lys^{177} (E177K) in HLA-A2 H chain and probed the association with E3-19K using a native gel band-shift assay (Fig. 4D). The results show that Ad4 and Ad2 E3-19K interact more weakly with HLA-A2(Q54G), relative to the control HLA-A2, as evidenced by the presence of residual uncomplexed HLA-A2(Q54G), the reduced intensities of the bands corresponding to complexes (more evident for Ad2 E3-19K), and the protein smear (more evident for Ad4 E3-19K). Furthermore, interaction of Ad4 and Ad2 E3-19K with HLA-A2 (E177K) failed to generate bands at the positions expected for complexes. This result is noteworthy given that Ad4 and Ad2 E3-19K mediate different types of interactions with E177: hydrophobic interactions for Ad4 E3-19K (Fig. 2) and salt bridges

for Ad2 E3-19K (31). Together, results from native gel analysis provide evidence that residue 54 and, especially, residue 177 in HLA-A2 H chain play important roles at the binding interface, consistent with our structural analysis.

Ad4 E3-19K/HLA-A2 and Ad2 E3-19K/HLA-A2 structures: insights into locus-specific interactions

The HCMV-encoded US2 protein, which also binds to HLA-A2 at the N-terminal end of the groove (51), does not interact with HLA-C molecules (35). To gain insights into the structural basis underlying the MHCI locus specificity of US2 and E3-19K, we mapped the binding surface of Ad4 E3-19K (yellow), Ad2 E3-19K (orange), and US2 (green) on HLA-A2 (Fig. 5A). The analysis shows that Ad4 E3-19K and US2 (Fig. 5A, left panel) share contact residue Glu^{177} (cyan), whereas Ad2 E3-19K and US2 (Fig. 5A, right panel) share residues Glu^{177} and Arg^{181} (cyan). As discussed above, Glu^{177} is critical for Ad4 and Ad2 E3-19K interaction with HLA-A2 (Fig. 4D), as well as HLA-A11 (33). Similarly, Arg^{181} was shown to be critical for Ad2 E3-19K and US2 function (19, 51). Remarkably, Fig. 5B shows that the side chain of Glu177 in HLA-Cw4 (PDB 1QQD) (blue) points in a different orientation relative to the orientations this residue adopts in its free and liganded HLA-A2 forms; compare free HLA-A2/Tax (PDB 1HHK) (magenta) with Ad4 E3-19K/HLA-A2 (yellow) and Ad2 E3-19K/HLA-A2 (orange). Taken together, this analysis points to the region of HLA-A2 in the vicinity of site 2 as playing a potential role in the MHCI locus specificity of these viral immunoevasins.

Discussion

Viruses have evolved specific mechanisms to interfere with the MHCI pathway and suppress Ag presentation. Ads encode the E3-19K protein that targets MHCI molecules for retention within the ER of infected cells. We determined the x-ray crystal structure of species E Ad4 E3-19K bound to HLA-A2, defined the mode of binding and contact sites, and compared the findings with those of our species C Ad2 E3-19K/HLA-A2 structure (31).

To function effectively as an immunomodulatory protein, the ER lumenal domain of E3-19K must establish "cross-reactive" and high-affinity interactions with the ER lumenal domain of MHCI molecules. First, Ad4 and Ad2 E3-19K proteins achieve functional promiscuity by contacting mostly conserved residues on HLA-A2, albeit not necessarily the same conserved residues, and by avoiding contacts with the bound antigenic peptide. Second, we showed that Ad4 and Ad2 E3-19K indeed bind tightly to HLA-A2 (Fig. 4D); we also previously determined a K_d of 12 nM for Ad2 E3-19K/HLA-A2 complex (32). Our structures show that, although both E3-19K proteins bind to the same hot spots on HLA-A2 (sites 1–4), overall, they mediate different types of interactions at sites 1–3 and more similar interactions at site 4. Indeed, relative to Ad2 E3-19K, Ad4 E3-19K establishes fewer

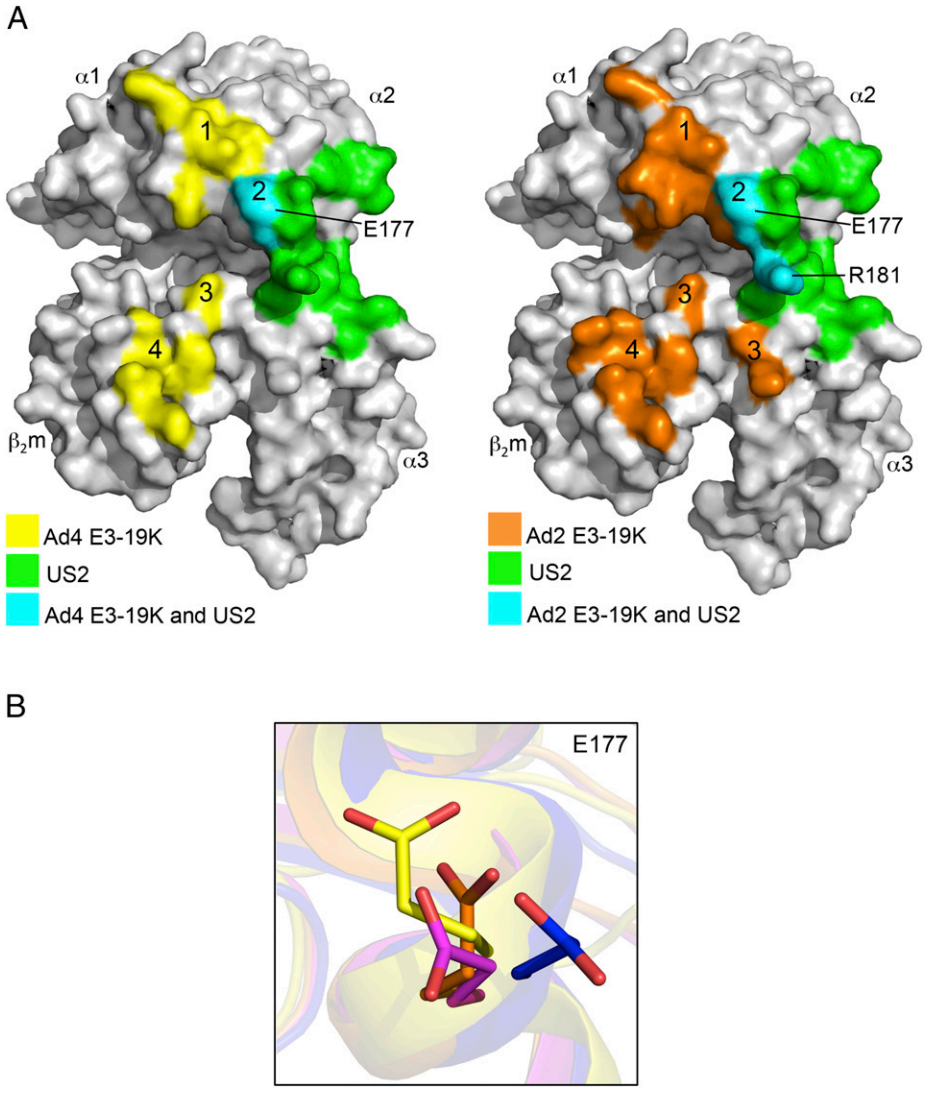

FIGURE 5. MHCI locus specificity of viral immunoevasins. (**A**) The binding surface of Ad4 E3-19K (yellow), Ad2 E3-19K (31) (orange), and US2 (51) (green) at sites 1–4 on HLA-A2 showing overlapping contact residues Glu^{177} and Arg^{181} (cyan). The α1-, α2-, and α3-domains of HLA-A2 H chain and β_2m are labeled. (**B**) The side chain orientation of Glu^{177} in the superimposed structures of free HLA-Cw4 (PDB 1QQD) (blue), free HLA-A2/Tax (PDB 1HHQ) (magenta), Ad4 E3-19K/HLA-A2 (yellow), and Ad2 E3-19K/HLA-A2 (orange).

hydrogen bonds and no salt bridges at sites 1–3 and instead relies extensively on hydrophobic contacts. These differences are not surprising given that Ad4 and Ad2 E3-19K use almost exclusively nonconserved residues to bind to HLA-A2 H chain at sites 1–3. In contrast, Ad4 and Ad2 E3-19K proteins use three strictly conserved residues (Met^{97}, Gln^{100}, and Tyr^{101}) to contact the same β_2m residues at site 4. Therefore, taken together, Ad4 and Ad2 E3-19K proteins achieve high-affinity binding from the energetic contribution of all interactions along their respective interfaces, including the conservation of extensive hydrophobic contacts at site 4. In addition, we suggest that shape complementarity plays a role in the favorable recognition of HLA-A2 by E3-19K proteins.

A role for shape complementarity at the interface of E3-19K/HLA-A2 complexes is supported by a number of observations. First, the Sc is reasonably high at all sites, with the exception of site 3, and is remarkably similar between the two E3-19K/HLA-A2 structures: site 1, Sc = 0.709 (Ad4) and 0.693 (Ad2) (31); site 2, Sc = 0.605 (Ad4) and 0.658 (Ad2); site 3, Sc = 0.333 (Ad4) and 0.341 (Ad2); and site 4, Sc = 0.799 (Ad4) and 0.801 (Ad2). Second, the binding interfaces of both E3-19K/HLA-A2 structures are characterized by relatively large buried surface area: 2112 $Å^2$ for Ad4 E3-19K/HLA-A2 and 1929 $Å^2$ for Ad2 E3-19K/HLA-A2 (31). Finally, we (32–34) showed that the mutation of even single contact residues in either E3-19K or MHCI can have global inhibitory effects on complex formation (Fig. 4D). Together, these observations are consistent with favorable shape complementarity at the E3-19K/HLA-A2 interfaces.

It is interesting to note that, in both Ad4 and Ad2 E3-19K/HLA-A2 structures, the Sc values are highest at site 4 (see Sc values above). Site 4 is particularly striking in that it involves an extended network of hydrophobic contacts between a few strictly conserved residues of the E3-19K α helix, one of the most conserved regions of E3-19K proteins across Ad species (Supplemental Fig. 1), and residues of β_2m (Fig. 2) (31). Another noticeable feature of both structures is the pronounced backbone curvatures of the E3-19K C terminus tails. The curvatures arise from internal packing interactions involving the strictly conserved WPP motif (Supplemental Fig. 1). As we reported previously (31), the proline residues of the WPP motif likely provide conformational rigidity to the tail, reducing conformational freedom of the membrane-anchored ER lumenal domain of E3-19K. Therefore, the strictly conserved WPP motif may serve to correctly orient the ER lumenal domain of E3-19K and initiate some favorable recognition event with HLA-A2, perhaps between the membrane-proximal E3-19K α helix and β_2m (site 4), as a starting point that drives interactions at the other three sites.

It is also interesting to note that, in both Ad4 and Ad2 E3-19K/HLA-A2 structures, the Sc values are lowest at site 3 (see Sc values above); this may be because interactions at site 3 involve residues on flexible loops of E3-19K and HLA-A2 α3-domain (Fig. 2) (31). Another distinct feature of site 3 is that it involves a region of HLA-A2 where the consensus sequences of HLA H chains are most divergent (Fig. 3A). Together, these characteristics likely contribute to why interactions at site 3, more than at any other site, are distinctively different between the two structures. It is likely that these differences contribute to the differential binding affinities that E3-19K proteins of different Ad species have for a given MHCI molecule.

E3-19K proteins selectively associate with MHCI molecules, recognizing HLA-A and HLA-B molecules but not HLA-C molecules. No study has explained, at the molecular level, how viral immunomodulatory proteins discriminate between seemingly similar MHCI molecules. In our analysis of Fig. 5A, we identified that Glu^{177} on HLA-A2 H chain is a common contact for Ad4 E3-19K, Ad2 E3-19K, and HCMV US2, which all discriminate against HLA-C, whereas Arg^{181} is common to Ad2 E3-19K and HCMV US2. We also showed that the side chain of Glu^{177} is oriented differently in free HLA-Cw4 in comparison with free HLA-A2/Tax and that there is minimal movement of this side chain upon formation of E3-19K/HLA-A2 complexes. Therefore, the region surrounding residues 177 and 181 on HLA H chains can potentially have a role in defining the binding specificity of E3-19K proteins for MHCI molecules.

A comparative analysis of Ad4 and Ad2 E3-19K/HLA-A2 structures reveals other notable features. At site 1, although Ad4 E3-19K uses Trp^{37} to make numerous hydrophobic contacts with the backbone of Gly^{56} at the tip of α1 helix (Fig. 2A), Ad2 E3-19K uses Tyr^{46} on a different loop to mediate similar interactions with Gly^{56} (31). Because we showed previously that residue 56 is critically important for the recognition of MHCI by Ad2 E3-19K (32), it is clear that different E3-19K proteins find different ways of maintaining interactions with MHC residue 56. An examination of the amino acid sequences of E3-19K proteins of species B and D at position 37 (Supplemental Fig. 1) shows that they carry Trp and His, respectively; in contrast, those of species C carry Thr. Therefore, these facts, together with other structural points discussed above, make the Ad4 E3-19K/HLA-A2 structure, rather than the Ad2 E3-19K/HLA-A2 structure, a more universal structure to make predictions on how E3-19K proteins of species B and D interact with HLA-A2. However, in this regard, it is worth mentioning that E3-19K proteins of species D are distinctively different from all other species in that they have several divergent amino acids in the α helix (Supplemental Fig. 1), including nonconserved substitutions at the three contact residues: Met^{97}, Gln^{100}, and Tyr^{101}. These differences in species D E3-19K proteins are likely to impair interactions between α helix residues and β_2m residues, as seen at site 4 in our structures (Fig. 2) (31). Consistent with this, Ad37 E3-19K of species D has a very low affinity for HLA-A molecules, and no measurable affinity for HLA-B molecules, relative to E3-19K proteins of species B, C, and E (33). Determining the x-ray structure of a species D E3-19K protein bound to HLA-A2 would be highly valuable in revealing interactions in a low-affinity complex.

Overall, our study provides a structural understanding of how two E3-19K proteins of different Ad species, Ad4 E3-19K of species E and Ad2 E3-19K of species C, with low levels of amino acid sequence homologies nonetheless share the same tertiary fold and MHCI-binding function. The conservation of these features underscores a critical role for E3-19K proteins in the pathogenesis of Ads. This is corroborated by the fact that species D Ads have evolved a unique immunomodulatory protein, E3/49K protein, which binds to CD45 to suppress the functions of T cells and NK cells (52, 53). This evasion mechanism may have been evolved by species D partly because of the low binding affinity that their E3-19K proteins have for MHCI molecules, as discussed above. Overall, our structural findings help to better understand the molecular basis by which Ad counteracts cellular immune defenses for survival inside host cells.

Acknowledgments

We thank Yasameen Muzahim for technical help and Dr. Karl Volz for discussions. We also thank the Argonne National Laboratory for beam time and staff support.

Disclosures

The authors have no financial conflicts of interest.

References

1. Wadell, G. 1984. Molecular epidemiology of human adenoviruses. *Curr. Top. Microbiol. Immunol.* 110: 191–220.

2. Berk, A. J. 2007. Adenoviridae: the viruses and their replication. In *Fields Virology*, 5th Ed. D. M. Knipe, and P. M. Howley, eds. Lippincott Williams & Wilkins, Philadelphia, p. 2355–2394.
3. Hage, E., U. Gerd Liebert, S. Bergs, T. Ganzenmueller, and A. Heim. 2015. Human mastadenovirus type 70: a novel, multiple recombinant species D mastadenovirus isolated from diarrhoeal faeces of a haematopoietic stem cell transplantation recipient. *J. Gen. Virol.* 96: 2734–2742.
4. Horwitz, M. S. 1990. Adenoviridae and their replication. In *Virology*, 2nd Ed. B. N. Fields, and D. M. Knipe, eds. Raven Press, New York, p. 1723–1740.
5. Hierholzer, J. C. 1992. Adenoviruses in the immunocompromised host. *Clin. Microbiol. Rev.* 5: 262–274.
6. Flomenberg, P., J. Babbitt, W. R. Drobyski, R. C. Ash, D. R. Carrigan, G. V. Sedmak, T. McAuliffe, B. Camitta, M. M. Horowitz, N. Bunin, and J. T. Casper. 1994. Increasing incidence of adenovirus disease in bone marrow transplant recipients. *J. Infect. Dis.* 169: 775–781.
7. Zahradnik, J. M., M. J. Spencer, and D. D. Porter. 1980. Adenovirus infection in the immunocompromised patient. *Am. J. Med.* 68: 725–732.
8. Krilov, L. R., L. G. Rubin, M. Frogel, E. Gloster, K. Ni, M. Kaplan, and S. M. Lipson. 1990. Disseminated adenovirus infection with hepatic necrosis in patients with human immunodeficiency virus infection and other immunodeficiency states. *Rev. Infect. Dis.* 12: 303–307.
9. Kosulin, K., E. Geiger, A. Vecsei, W. D. Huber, M. Rauch, E. Brenner, F. Wrba, K. Hammer, A. Innerhofer, U. Potschger, et al. 2016. Persistence and reactivation of human adenoviruses in the gastrointestinal tract. *Clin. Microbiol. Infect.* 22 (4): 381.e1–8. doi: 10.1016/j.cmi.2015.12.013.
10. Kvist, S., L. Ostberg, H. Persson, L. Philipson, and P. A. Peterson. 1978. Molecular association between transplantation antigens and cell surface antigen in adenovirus-transformed cell line. *Proc. Natl. Acad. Sci. USA* 75: 5674–5678.
11. Burgert, H.-G., and S. Kvist. 1985. An adenovirus type 2 glycoprotein blocks cell surface expression of human histocompatibility class I antigens. *Cell* 41: 987–997.
12. Pääbo, S., B. M. Bhat, W. S. M. Wold, and P. A. Peterson. 1987. A short sequence in the COOH-terminus makes an adenovirus membrane glycoprotein a resident of the endoplasmic reticulum. *Cell* 50: 311–317.
13. Cox, J. H., J. W. Yewdell, L. C. Eisenlohr, P. R. Johnson, and J. R. Bennink. 1990. Antigen presentation requires transport of MHC class I molecules from the endoplasmic reticulum. *Science* 247: 715–718.
14. Cox, J. H., J. R. Bennink, and J. W. Yewdell. 1991. Retention of adenovirus E19 glycoprotein in the endoplasmic reticulum is essential to its ability to block antigen presentation. *J. Exp. Med.* 174: 1629–1637.
15. Burgert, H.-G., and S. Kvist. 1987. The E3/19K protein of adenovirus type 2 binds to the domains of histocompatibility antigens required for CTL recognition. *EMBO J.* 6: 2019–2026.
16. Liu, H., W. F. Stafford, and M. Bouvier. 2005. The endoplasmic reticulum lumenal domain of the adenovirus type 2 E3-19K protein binds to peptide-filled and peptide-deficient HLA-A*1101 molecules. *J. Virol.* 79: 13317–13325.
17. Beier, D. C., J. H. Cox, D. R. Vining, P. Cresswell, and V. H. Engelhard. 1994. Association of human class I MHC alleles with the adenovirus E3/19K protein. *J. Immunol.* 152: 3862–3872.
18. Feuerbach, D., S. Etteldorf, C. Ebenau-Jehle, J.-P. Abastado, D. Madden, and H.-G. Burgert. 1994. Identification of amino acids within the MHC molecule important for the interaction with the adenovirus protein E3/19K. *J. Immunol.* 153: 1626–1636.
19. Flomenberg, P., E. Gutierrez, and K. T. Hogan. 1994. Identification of class I MHC regions which bind to the adenovirus E3-19k protein. *Mol. Immunol.* 31: 1277–1284.
20. Gabathuler, R., F. Lévy, and S. Kvist. 1990. Requirements for the association of adenovirus type 2 E3/19K wild-type and mutant proteins with HLA antigens. *J. Virol.* 64: 3679–3685.
21. Hermiston, T. W., R. A. Tripp, T. Sparer, L. R. Gooding, and W. S. M. Wold. 1993. Deletion mutation analysis of the adenovirus type 2 E3-gp19K protein: identification of sequences within the endoplasmic reticulum lumenal domain that are required for class I antigen binding and protection from adenovirus-specific cytotoxic T lymphocytes. *J. Virol.* 67: 5289–5298.
22. Flomenberg, P., J. Szmulewicz, E. Gutierrez, and H. Lupatkin. 1992. Role of the adenovirus E3-19k conserved region in binding major histocompatibility complex class I molecules. *J. Virol.* 66: 4778–4783.
23. Sester, M., Z. Ruszics, E. Mackley, and H.-G. Burgert. 2013. The transmembrane domain of the adenovirus E3/19K protein acts as an endoplasmic reticulum retention signal and contributes to intracellular sequestration of major histocompatibility complex class I molecules. *J. Virol.* 87: 6104–6117.
24. Flomenberg, P., V. Piaskowski, R. L. Truitt, and J. T. Casper. 1996. Human adenovirus-specific CD8+ T-cell responses are not inhibited by E3-19K in the presence of gamma interferon. *J. Virol.* 70: 6314–6322.
25. Andersson, M., A. McMichael, and P. A. Peterson. 1987. Reduced allorecognition of adenovirus-2 infected cells. *J. Immunol.* 138: 3960–3966.
26. Burgert, H.-G., J. L. Maryanski, and S. Kvist. 1987. "E3/19K" protein of adenovirus type 2 inhibits lysis of cytolytic T lymphocytes by blocking cell-surface expression of histocompatibility class I antigens. *Proc. Natl. Acad. Sci. USA* 84: 1356–1360.
27. Tanaka, Y., and S. S. Tevethia. 1988. Differential effect of adenovirus 2 E3/19K glycoprotein on the expression of H-2Kb and H-2Db class I antigens and H-2Kb- and H-2Db-restricted SV40-specific CTL-mediated lysis. *Virology* 165: 357–366.
28. Rawle, F. C., A. E. Tollefson, W. S. Wold, and L. R. Gooding. 1989. Mouse anti-adenovirus cytoxic T lymphocytes. Inhibition of lysis by E3 gp19K but not E3 14.7K *J. Immunol.* 143: 2031–2037.
29. Ginsberg, H. S., U. Lundholm-Beauchamp, R. L. Horswood, B. Pernis, W. S. Wold, R. M. Chanock, and G. A. Prince. 1989. Role of early region 3 (E3) in pathogenesis of adenovirus disease. *Proc. Natl. Acad. Sci. USA* 86: 3823–3827.
30. Ginsberg, H. S., L. L. Moldawer, P. B. Sehgal, M. Redington, P. L. Kilian, R. M. Chanock, and G. A. Prince. 1991. A mouse model for investigating the molecular pathogenesis of adenovirus pneumonia. *Proc. Natl. Acad. Sci. USA* 88: 1651–1655.
31. Li, L., Y. Muzahim, and M. Bouvier. 2012. Crystal structure of adenovirus E3-19K bound to HLA-A2 reveals mechanism for immunomodulation. *Nat. Struct. Mol. Biol.* 19: 1176–1181.
32. Liu, H., J. Fu, and M. Bouvier. 2007. Allele- and locus-specific recognition of class I MHC molecules by the immunomodulatory E3-19K protein from adenovirus. *J. Immunol.* 178: 4567–4575.
33. Fu, J., L. Li, and M. Bouvier. 2011. Adenovirus E3-19K proteins of different serotypes and subgroups have similar, yet distinct, immunomodulatory functions toward major histocompatibility class I molecules. *J. Biol. Chem.* 286: 17631–17639.
34. Fu, J., and M. Bouvier. 2011. Determinants of the endoplasmic reticulum (ER) lumenal-domain of the adenovirus serotype 2 E3-19K protein for association with and ER-retention of major histocompatibility complex class I molecules. *Mol. Immunol.* 48: 532–538.
35. Gewurz, B. E., E. W. Wang, D. Tortorella, D. J. Schust, and H. L. Ploegh. 2001. Human cytomegalovirus US2 endoplasmic reticulum-lumenal domain dictates association with major histocompatibility complex class I in a locus-specific manner. *J. Virol.* 75: 5197–5204.
36. Machold, R. P., E. J. Wiertz, T. R. Jones, and H. L. Ploegh. 1997. The HCMV gene products US11 and US2 differ in their ability to attack allelic forms of murine major histocompatibility complex (MHC) class I heavy chains. *J. Exp. Med.* 185: 363–366.
37. Cohen, G. B., R. T. Gandhi, D. M. Davis, O. Mandelboim, B. K. Chen, J. L. Strominger, and D. Baltimore. 1999. The selective downregulation of class I major histocompatibility complex proteins by HIV-1 protects HIV-infected cells from NK cells. *Immunity* 10: 661–671.
38. Le Gall, S., L. Erdtmann, S. Benichou, C. Berlioz-Torrent, L. Liu, R. Benarous, J. M. Heard, and O. Schwartz. 1998. Nef interacts with the mu subunit of clathrin adaptor complexes and reveals a cryptic sorting signal in MHC I molecules. *Immunity* 8: 483–495.
39. Ishido, S., J. K. Choi, B. S. Lee, C. Wang, M. DeMaria, R. P. Johnson, G. B. Cohen, and J. U. Jung. 2000. Inhibition of natural killer cell-mediated cytotoxicity by Kaposi's sarcoma-associated herpesvirus K5 protein. *Immunity* 13: 365–374.
40. Garboczi, D. N., D. T. Hung, and D. C. Wiley. 1992. HLA-A2-peptide complexes: refolding and crystallization of molecules expressed in *Escherichia coli* and complexed with single antigenic peptides. *Proc. Natl. Acad. Sci. USA* 89: 3429–3433.
41. Otwinowski, Z., and W. Minor. 1997. Processing of x-ray diffraction data collected in oscillation mode. In *Methods in Enzymology: Macromolecular Crystallography*, Part A, Vol. 276. C. W. Carter, Jr. and R. M. Sweet, eds. Academic Press, New York, p. 307–326. doi:10.1016/S0076-6879(97)76066-X.
42. Navaza, J. 1994. AMoRe: an automated package for molecular replacement. *Acta Crystallogr. A* 50: 157–163.
43. Murshudov, G. N., A. A. Vagin, and E. J. Dodson. 1997. Refinement of macromolecular structures by the maximum-likelihood method. *Acta Crystallogr. D Biol. Crystallogr.* 53: 240–255.
44. Emsley, P., and K. Cowtan. 2004. Coot: model-building tools for molecular graphics. *Acta Crystallogr. D Biol. Crystallogr.* 60: 2126–2132.
45. Afonine, P. V., R. W. Grosse-Kunstleve, N. Echols, J. J. Headd, N. W. Moriarty, M. Mustyakimov, T. C. Terwilliger, A. Urzhumtsev, P. H. Zwart, and P. D. Adams. 2012. Towards automated crystallographic structure refinement with phenix.refine. *Acta Crystallogr. D Biol. Crystallogr.* 68: 352–367.
46. Laskowski, R. A., M. W. MacArthur, D. S. Moss, and J. M. Thornton. 1993. PROCHECK: A program to check the stereochemical quality of protein structures. *J. Appl. Cryst.* 26: 283–291.
47. Schrödinger, LLC. 2010. The PyMOL molecular graphics system, version 1.4.1. Schrödinger, LLC, Portland, OR. http://www.pymol.org/pymol.
48. Guex, N., and M. C. Peitsch. 1997. SWISS-MODEL and the Swiss-PdbViewer: an environment for comparative protein modeling. *Electrophoresis* 18: 2714–2723.
49. Lawrence, M. C., and P. M. Colman. 1993. Shape complementarity at protein/protein interfaces. *J. Mol. Biol.* 234: 946–950.
50. Sester, M., and H.-G. Burgert. 1994. Conserved cysteine residues within the E3/19K protein of adenovirus type 2 are essential for binding to major histocompatibility complex antigens. *J. Virol.* 68: 5423–5432.
51. Gewurz, B. E., R. Gaudet, D. Tortorella, E. W. Wang, H. L. Ploegh, and D. C. Wiley. 2001. Antigen presentation subverted: Structure of the human cytomegalovirus protein US2 bound to the class I molecule HLA-A2. *Proc. Natl. Acad. Sci. USA* 98: 6794–6799.
52. Windheim, M., J. H. Southcombe, E. Kremmer, L. Chaplin, D. Urlaub, C. S. Falk, M. Claus, J. Mihm, M. Braithwaite, K. Dennehy, et al. 2013. A unique secreted adenovirus E3 protein binds to the leukocyte common antigen CD45 and modulates leukocyte functions. *Proc. Natl. Acad. Sci. USA* 110: E4884–E4893.
53. Windheim, M., S. Höning, K. N. Leppard, L. Butler, C. Seed, S. Ponnambalam, and H.-G. Burgert. 2016. Sorting motifs in the cytoplasmic tail of the immunomodulatory E3/49K protein of species D adenoviruses modulate cell surface expression and ectodomain shedding. *J. Biol. Chem.* 291: 6796–6812.